Segregation, transport, and interaction of climate proxies in polycrystalline ice

A.W. Rempel and J.S. Wettlaufer

Abstract: The most detailed records of the Earth's climate during the past few hundred millennia are derived from ice cores retrieved from Greenland and Antarctica. The analyses of these records assume that the distributions of the trace constituents that are used as proxies for past climate have not significantly altered since deposition at the surface, and yet careful studies, at high spatial resolution, have identified core segments where appreciable post-depositional changes have occurred. To improve the reliability and resolution of paleoclimate interpretations, we have examined the mechanisms underlying the transport and interaction of climate proxies in polycrystalline ice, many of which are soluble impurities that are found principally in premelted liquid that lines the boundaries between ice grains. We find that the rate of post-depositional alteration depends critically on where the trace constituents reside; whether in the premelted liquid, in which case they exert a controlling influence on the total volume fraction of liquid that is present, or in the grains themselves. In the former case, the premelted liquid reservoir contains the principle conduits through which many of the impurities are transported and interact, and in the latter case, the temporal evolution of impurity concentration is both slower and more complex. We provide quantitative models that describe these processes and highlight the importance of impurity segregation for our understanding of past climates.

PACS Nos.: 66.30Jt, 91.60Ed, 92.40Sn, 92.40Vq, 92.70-j

Résumé : Le meilleur registre que nous ayons du climat des dernières centaines de milliers d'années se trouve dans les carottes de glace retirées des glaciers du Groenland et de l'Antarctique. L'analyse de ces carottes suppose que la distribution des éléments en trace (impuretés de faible concentration) utilisés comme indicateurs des climats passés n'a pas changé significativement depuis leur dépôt en surface. Néanmoins, des études minutieuses à haute résolution saptiale ont identifié des segments de carotte où apparaissent des variations post-dépôt significatives de concentration de ces éléments. Afin d'améliorer la fiabilité et la résolution des interprétations paléoclimatiques, nous avons étudié les mécanismes responsables du transport et de l'interaction des éléments indicateurs dans de la glace polycristalline, dont plusieurs sont des impuretés solubles retrouvées surtout dans les liquides de pré-fonte qui couvrent les interfaces entre les cristaux de glace. Nous trouvons que le

Received 15July 2002. Accepted 28 October 2002. Published on the NRC Research Press Web site at http://cjp.nrc.ca/ on 19 March 2003.

A.W. Rempel.[1] Department of Geology and Geophysics, Yale University, New Haven, CT 06520-8109, U.S.A.
J.S. Wettlaufer. Department of Geology and Geophysics, Yale University, New Haven, CT 06520-8109, U.S.A. and Department of Physics, Yale University, New Haven, CT 06520-8120, U.S.A.

[1]Corresponding author (e-mail: alan.rempel@yale.edu).

 doi: 10.1139/P02-118

taux d'altération post-dépôt dépend de façon critique de l'endroit où les impuretés résident : soit dans le liquide de pré-fonte, auquel cas ils contrôlent la fraction totale du volume de liquide, soit dans les cristaux eux-mêmes. Dans le premier cas, le réservoir de liquide de pré-fonte fournit les conduits principaux où les impuretés migrent et interagissenent. Dans le dernier cas, l'évolution temporelle des concentrations est plus lente et plus complexe. Nous proposons des modèles quantitatifs de ces mécanismes et soulignons l'importance de séparer les impuretés dans notre compréhension des climats passés.

[Traduit par la Rédaction]

1. Introduction

Ice cores retrieved from the polar ice sheets contain high-resolution, long-term ($>10^5$ years) archives of trace constituents that are transported from the glacier surface with the flowing and deforming polycrystalline ice [1,2]. Vertical variations in the measured constituent profiles reflect the temporal variations in their pattern of deposition that were caused by changing climate conditions. To accurately interpret these valuable records of past climate, care must be taken to account for processes that have altered the spatial distribution of the climate proxies during their long residence in the ice sheets prior to core recovery. For example, in the uppermost 50–150 m the vapour between ice grains forms connected pathways that allow rapid gas diffusion, which leads to an age offset between the ice and the paleoatmospheric samples retrieved later from bubbles and clathrate crystals [3]. Compaction and recrystallization seal the vapour pores so that they no longer form connected fluid networks lower down in the ice sheets. However, *premelted* liquid that traces the boundaries between ice grains represents a key fluid reservoir that can "short-circuit" sluggish solid-state diffusion and facilitate interactions between trace constituents [4–7]. Many of these constituents are soluble impurities that exert a dominant influence on the volume fraction of premelted liquid that is available to enhance rates of post-depositional change [8]. We examine the interactions between soluble impurities and the phase behaviour of ice to provide a framework for evaluating the degree to which these trace-constituent records have been altered during the time since deposition.

2. Equilibrium requirements

The coexistence between a liquid and its solid at temperatures T that are lower than the normal melting temperature of the bulk, T_{m}, is a basic aspect of the phase behaviour of most solids, including ice, known as *premelting* [9,10]. Perhaps the most familiar cause of premelting is the presence of soluble impurities, which lower the chemical potential of the liquid to a degree that depends on their concentration c_i in solution. At temperatures that are above eutectic for an aqueous solution that contains N distinct species, the effects of impurities are often well-described over modest ranges in temperature and composition with a linear function of the intergranular concentrations c_i — defined here as the number of moles of the ith impurity divided by the volume of solution in which they are dissolved. In practice, empirical, nonlinear relationships between T and c_i may be necessary for quantitative comparison between theory and observations from specific core sections, such complications are easily incorporated into the model described here and do not alter its essential features. In addition to the effects of impurities, for a solid–liquid interface with curvature $\mathcal{K}$, the Gibbs–Thomson effect describes how the surface energy σ_{sl} contributes to the departure of the equilibrium temperature from that at bulk coexistence. When a solid is in close proximity to a substrate, such as another solid grain, a dust particle, or a bubble of vapour, intermolecular interactions can also cause a premelted film of liquid to form and separate their surfaces by a distance d that is inversely related to the disjoining pressure p_T. Taking each of these effects into account, the equilibrium condition in a system with N impurity species present is

$$T_{\mathrm{m}} - T = \sum_{i=1}^{N} \Gamma_i c_i + \frac{T_{\mathrm{m}}\sigma_{\mathrm{sl}}}{\rho_{\mathrm{s}} q_{\mathrm{m}}}\mathcal{K} + \frac{T_{\mathrm{m}}}{\rho_{\mathrm{s}} q_{\mathrm{m}}} p_T(d) \tag{1}$$

where Γ_i is the liquidus slope for the ith impurity species, $\rho_s = 917\ \mathrm{kg\,m^{-3}}$ is the density of ice, $q_m = 3.34 \times 10^5\ \mathrm{J\,kg^{-1}}$ is the latent heat of fusion, and $T_m \approx 273$ K is the bulk melting temperature at the in-situ ice pressure. Within ice sheets we expect all interfaces between solid ice and premelted liquid to satisfy (1).

2.1. Veins

Measured dihedral angles in polycrystalline ice are less than 60° [11]; this implies that melt channels, known as veins, run along the triple-junctions and join at nodes where four ice grains meet [12,13]. Similar in geometry to the plateau borders in a foam, the vein–node system forms a connected liquid network that can dominate the transport of material relative to the solid ice matrix. Along the solid–liquid interfaces that define the vein walls, the curvature is $\mathcal{K} = 1/R_v$, where R_v is the vein radius. Substrate interactions are weak along veins because the ice surfaces are distant in comparison to the range of intermolecular forces (except in the negligibly small regions close to grain boundaries at vein edges). As a lower bound, we define the characteristic radius

$$R_c \equiv \frac{T_m \sigma_{sl}}{\rho_s q_m (T_m - T)} \tag{2}$$

as the radius that a vein would have if no impurities were present. For physical intuition, we take $\sigma_{sl} \approx 0.035\ \mathrm{J\,m^{-2}}$ and note that $R_c \approx 3 \times 10^{-9}$ m when the temperature $T \approx 263$ K. Using (2), we rewrite (1) in the limit that $p_T(d)$ tends to zero and find that the equilibrium condition in the veins is

$$T_m - T = \sum_{i=1}^{N} \Gamma_i c_i + (T_m - T)\frac{R_c}{R_v} \tag{3}$$

While no precise measurements of R_v have been reported for polar glacier ice, indirect evidence from efforts to detect the microscopic locations of impurity molecules indicates that typically $R_v \gg R_c$ [7,14,15]. Hence, we can infer that the effect of interfacial curvature is negligible and the solute concentration in the veins is determined by the bulk-phase diagram, approximated here as

$$T_m - T = \sum_{i=1}^{N} \Gamma_i c_i \tag{4}$$

The temperature is routinely measured as a function of depth along core bore holes [16], so (4) can be used to determine the gradients in intergranular concentration that drive molecular diffusion through the veins.

3. Continuum models

Chemical analyses were performed on melt water derived from polycrystalline core samples [17,18], and reported as bulk concentration values c_{Bi} — defined here as the number of moles of the ith impurity species divided by the sample volume. Changes in the bulk concentrations record changes in the chemical loading that reflect climatic variability on a range of temporal scales, which can often be detected down to seasonal levels by careful, high-resolution analysis of ice cores [18]. As grains slowly grow and recrystallize within the ice sheet, most of the impurity molecules are preferentially excluded from the solid grains and enriched in the melt [19]. The polycrystalline mixture of ice and liquid solution flows downwards under gravity at velocity $\boldsymbol{v}$ and encounters gradual variations in temperature caused by the near-constant flux of geothermal heat and the increasingly damped response to oscillations in surface temperature. The shallow gradients in temperature lead to gradients in intergranular concentrations c_i that drive molecular diffusion of solutes relative to the ice matrix. We treat the polycrystalline ice as a continuum containing aqueous solution with volume fraction ϕ, and quantify the effects of diffusive transport on the c_{Bi} records.

3.1. Single species

We first consider the case where a single dissolved constituent dominates the phase behaviour so that $N = 1$ in (4) and $\nabla c \propto \nabla T$. When most of the impurity molecules are dissolved within the premelted liquid, the balance of species requires that $c_B \approx \phi c$. The solid ice matrix is treated as incompressible (i.e., $\nabla \cdot \boldsymbol{v} = 0$) and the flow of liquid relative to the ice is considered negligible. The condition for solute conservation in a moving polycrystalline volume Ω with surface element $\mathrm{d}\boldsymbol{S}$ is [6]

$$\frac{\partial}{\partial t}\int_{\Omega} \phi c \,\mathrm{d}\Omega = -\oint_{S} (\phi c \boldsymbol{v} - \phi D \nabla c) \cdot \mathrm{d}\boldsymbol{S} \tag{5}$$

where D is the effective molecular diffusivity through the liquid. (When the liquid pathways are randomly oriented with respect to the prevailing concentration gradient, D is reduced from the normal molecular diffusivity by a factor of 3 — an effect referred to as Lemlich's formula in the literature on foams [20].) We apply the divergence theorem and use (4) to rewrite (5) in terms of the measured variables c_B and T as

$$\frac{\partial}{\partial t} c_B = -\nabla \cdot \left(c_B \boldsymbol{v} + c_B D \frac{\nabla T}{T_m - T} \right) \tag{6}$$

noting that the integrating volume is arbitrary so the integrands must be equal. Measured variations in c_B occur over much shorter length scales than do variations in ∇T. Expanding the right side and retaining the dominant terms we find that

$$\frac{\partial}{\partial t} c_B \approx -(\boldsymbol{v} + \boldsymbol{v}_c) \cdot \nabla c_B \tag{7}$$

where the anomalous velocity is defined as

$$\boldsymbol{v}_c \equiv -D \frac{\nabla c}{c} = D \frac{\nabla T}{T_m - T} \tag{8}$$

and the second equality applies specifically to the case of a linear liquidus considered here. Equation (7) indicates that, while the ice matrix flows at velocity $\boldsymbol{v}$, compositional diffusion through the liquid causes the bulk-impurity profile to move at a rate that differs by a finite anomalous velocity $\boldsymbol{v}_c$ [6]. Over long time periods, this *anomalous diffusion* can cause bulk-impurity profiles to become separated from the ice and other climate proxies that they were deposited with, as illustrated in Fig. 1. This process should be taken into account to avoid errors in interpretations for the relative timing of paleoclimatic events. However, because the temperature gradients in ice sheets are generally shallow ($\nabla T = O\left(10^{-2}\right) \mathrm{K\,m^{-1}}$), expected anomalous velocities are typically less than 1 μm per year in the upper portions of ice sheets and significant displacement only occurs by this mechanism after relatively long time periods (see Fig. 1). Next, we examine how interactions within polycrystalline ice that contains multiple impurity species can lead to significant changes to climate-proxy records over much shorter times.

3.2. Multiple species

When several impurity species are in aqueous solution, each one contributes to lowering the chemical potential of the liquid and the total liquid fraction ϕ adjusts so that the intergranular concentrations satisfy (4). With N species present and most of each segregated to the liquid, the constituent balance requires that the bulk concentration for the ith component satisfies $c_{Bi} \approx \phi c_i$. The evolution of each bulk-concentration profile is described by [7]

$$\frac{\partial}{\partial t} c_{Bi} + \boldsymbol{v} \cdot c_{Bi} = -\nabla \cdot (\boldsymbol{v}_{ci} c_{Bi}) \tag{9}$$

Fig. 1. The continuous curve shows how the predicted separation between a soluble-impurity record and the ice with which it was deposited increases with depth beneath the glacial surface (adapted from ref. 6). The temperature profile and ice-flow parameters used for these calculations were based on contemporary conditions in the Greenland ice sheet at the location where the GRIP ice core was drilled; the liquidus slope was based on the phase diagram for H_2SO_4 solutions. By 2800 m depth the predicted separation reaches 0.5 m, which is a distance that corresponds to an apparent time difference of approximately one century. In other words, the model predicts that an ice parcel at that depth accumulated on the surface one century earlier than the impurities that are now contained in its melt. The broken line shows the predicted anomalous velocities used to calculate the separation, labelled in units of metres per year on the upper axis. The axis on the right shows the undercooling $T_m - T$ at 200 m depth increments.

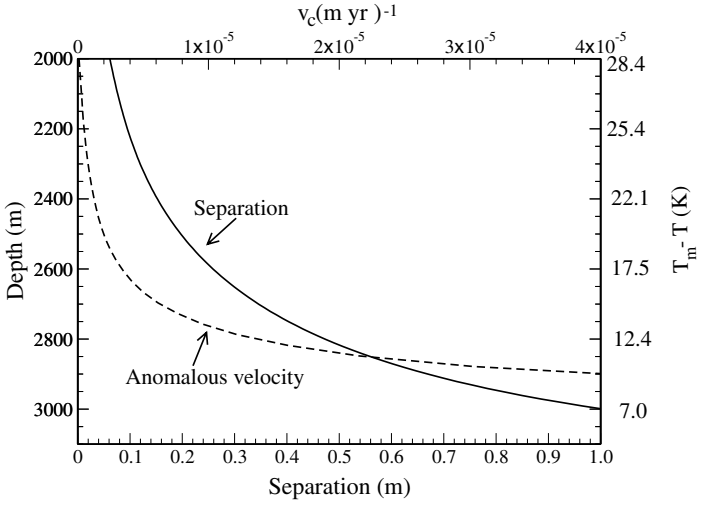

where the anomalous velocity is

$$\boldsymbol{v}_{ci} \equiv -D_i \frac{\nabla c_i}{c_i} = D_i \left(\frac{\nabla T}{T_m - T} + \frac{\sum_{j=1}^{N} \Gamma_j \nabla c_{Bj} - \frac{\nabla c_{Bi}}{c_{Bi}} \sum_{j=1}^{N} \Gamma_j c_{Bj}}{\sum_{j=1}^{N} \Gamma_j c_{Bj}} \right) \tag{10}$$

When the bulk concentrations co-vary, the ratio c_{Bi}/c_{Bj} is spatially uniform for each combination of impurities i and j and the second term in parentheses is zero; in this case, each anomalous velocity is proportional to the temperature gradient and anomalous diffusion produces the same behaviour as described above for the single-species case. When there are spatial variations in the relative proportions of the constituent species, however, these produce gradients in the intergranular concentrations that drive diffusive transport at rates that vary along each constituent profile on length scales that are commensurate with those for variations in c_{Bi}. To illustrate how the bulk-impurity profiles are altered by the resulting diffusive transport, in Fig. 2 we show the isothermal evolution of two sinusoidal profiles that are initially asynchronous [7]. Since typical liquidus slopes, Γ_1 and Γ_2, are similar in size, this implies that the volume fraction of liquid is largest where the chemical loading is greatest. In this example c_{B2} is always much greater than c_{B1} so peaks in ϕ correspond to maxima in c_{B2}. Compositional diffusion acts to eliminate the intergranular concentration gradients, and causes the peak in c_{B1} to shift to become in phase with the peak in c_{B2}; one species is a slave to the other. A steady state is reached once the profiles achieve a spatially-uniform ratio of c_{B1}/c_{B2}. Similar behaviour has been noted at several coastal Antarctic stations, where peak concentrations of methane sulfonic acid (derived from marine biogenic activity) that are deposited during Austral summers migrate to become in phase with peaks in sea-salt concentrations that are deposited during the winter [18]. Our model shows how composition diffusion alone can explain the redistribution of peaks in the bulk concentrations of climate proxies. Interestingly, peaks in sulfate concentration, which are deposited primarily in phase with the methane sulfonic acid, appear not to be subject to this redistribution mechanism; this highlights the importance of other processes that have not

Fig. 2. The isothermal evolution of periodic c_{Bi} profiles that were deposited asynchronously on the surface of an ice sheet (adapted from ref. 7); note the different scales for c_{B1} and c_{B2} on the left and right axes. The horizontal axis represents the distance along the core, measured in terms of the period of the anomaly cycle. The heavy dotted–broken lines show the initial profiles and the broken lines show the profiles at subsequent times. The continuous lines show the steady state that is achieved once the low-amplitude c_{B1} profile is in phase with the c_{B2} profile, which is not significantly altered.

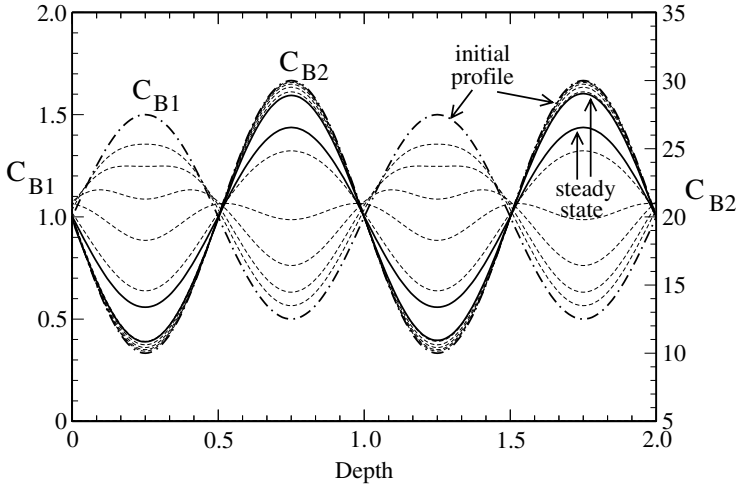

yet been incorporated in this model.

3.3. Segregated species

In addition to being dissolved in the vein network, impurity species can also be concentrated on the surfaces of grain boundaries, dust particles, air bubbles, and clathrate crystals. Moreover, although most impurity molecules are too large to form substitutional defects within the ice lattice, it has been suggested that they might nevertheless be present in the solid grains [21–23], presumably at other point defects such as interstitials and vacancies. For the present analysis, we assume that the impurity molecules are able to exchange rapidly between the various microscopic reservoirs so that the impurity distribution is maintained in local equilibrium on the time scale of the macroscopic signal alterations. When a significant fraction of the total impurity content is not contained in the connected porosity ϕ, we can write

$$c_{Bi} = c_i\,(\phi + k_{ei}) \tag{11}$$

where the effective distribution coefficient k_{ei} accounts for the impurity molecules that are not dissolved in the liquid network.

We can describe the species balance by considering the geometrical constraints on the relative proportions of impurities that are present in each potential reservoir. For example, consider a polycrystalline sample with grain size b that contains veins of radius R_v, having intergranular concentration c_i. The total impurity content in each grain is proportional to $c_{Bi}b^3$ and the quantity of impurities contained in the surrounding veins is proportional to $c_i b R_v^2$. The grain boundaries have an effective film thickness d_f and impurity concentration c_{fi} so that $c_{fi}d_f$ is the number of moles of impurity i divided by the grain-boundary surface area, which is proportional to b^2. The sample contains solid particles in number density n_p with radii R_p and surface-impurity concentration $c_{pi}d_p$. Bubbles or clathrate crystals are present with number density n_b, radii R_b and surface-impurity concentration $c_{bi}d_b$. We assume that the molar concentration of the ith impurity in the solid grains themselves c_{gi} is proportional to the intergranular concentration in the veins through a distribution coefficient $k_{gi} \equiv c_{gi}/c_i$. The balance

Fig. 3. The isothermal evolution of the same initial c_{Bi} profiles as were shown in Fig. 2, but with a significant fraction of both impurity species segregated from the melt. The ratios of the effective distribution coefficients k_{ei} to the porosity ϕ vary spatially from a maximum of 100 where c_{B2} is lowest, to a minimum of approximately 0.5 at the peaks in c_{B2}. The broken lines showing the evolving c_{B1} profile retain the initial peak for much longer than in the case displayed in Fig. 2, where $k_{ei} \ll \phi$. These are the locations of porosity minima, where the effects of segregation slow anomalous diffusion to the greatest extent.

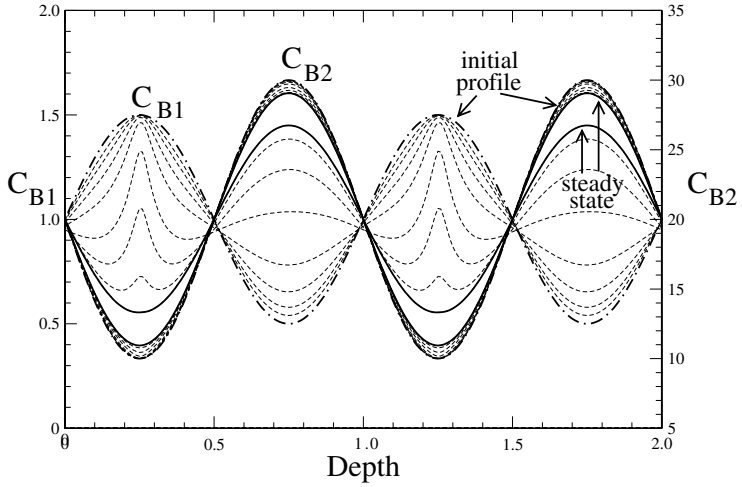

condition for the ith impurity species is

$$c_{Bi} = \alpha_v c_i \left(\frac{R_v}{b}\right)^2 + \alpha_f c_{fi} \frac{d_f}{b} + \alpha_p c_{pi} d_p R_p^2 n_p + \alpha_b c_{bi} d_b R_b^2 n_b + k_{gi} c_i \tag{12}$$

where α_v, α_f, α_p, and α_b are geometrical factors of order unity. When intermolecular interactions cause liquid films to form on grain boundaries, particles, and bubbles, and compositional diffusion equilibrates the solute concentrations with those in the veins, we have $c_i = c_{fi} = c_{pi} = c_{bi}$. In this case the porosity is $\phi = \alpha_v (R_v/b)^2 + \alpha_f (d_f/b) + \alpha_p d_p R_p^2 n_p + \alpha_b d_b R_b^2 n_b$ and the effective distribution coefficient in (11) is $k_{ei} = k_{gi}$. Alternatively, if the impurities on grain boundaries, particles, and bubbles are not in solution or are prevented from reaching the same intergranular composition as the veins, we can define the effective distribution coefficient as $k_{ei} = k_{gi} + \alpha_f (d_f/b)(c_{fi}/c_i) + \alpha_p d_p R_p^2 n_p (c_{pi}/c_i) + \alpha_b d_b R_b^2 n_b (c_{bi}/c_i)$ and write the porosity as $\phi \equiv \alpha_v (R_v/b)^2$ so that the constituent balance still satisfies (11). Appropriate definitions for ϕ and k_{ei} that are consistent with (11) and (12) can also be made for other segregation scenarios that are intermediate between these two end members. Efforts to detect the microscopic distribution of impurities in polar ice samples [14,15,22–25] hold promise for better constraining the appropriate functional dependence of k_{ei} and ϕ on core-sample characteristics.

The evolution of each bulk concentration profile is described by (9) when (11) holds, but with the generalized anomalous velocity defined as

$$\boldsymbol{v}_{ci} \equiv -D_i \frac{\nabla c_i}{c_i} \left(1 + \frac{k_{ei}}{\phi}\right)^{-1} \tag{13}$$

Most of the impurities are dissolved in solution when $\phi \gg k_{ei}$ and $\boldsymbol{v}_{ci} \approx -D_i \nabla c_i / c_i$ as before. However, when the distribution coefficient is comparable to or greater than ϕ, the anomalous velocity is reduced and the bulk-impurity profile evolves more slowly. Moreover, since the anomalous velocity depends on the ratio of k_{ei}/ϕ, the rate at which the impurity profile evolves is altered by segregation to a greater extent at locations where the porosity is lower. In Fig. 3 we show the evolution of the periodic bulk-concentration profiles considered in Fig. 2, but with each species characterized by a constant distribution

coefficient that is one hundred times greater than the minimum initial porosity and only half as large as the maximum initial porosity. The signals evolve to the same steady state as before, but at different *rates* along the profiles. At intermediate times the c_{B1} profiles, in particular, are considerably altered from those displayed in Fig. 2. Further analysis shows that when the effective distribution coefficients of the dissolved impurity species are not equal to each other, the isothermal steady-state distributions are also modified so that c_{B1}/c_{B2} no longer tends to a spatially-uniform value. This suggests the potential for using high-resolution core analyses in conjunction with different modelling scenarios to invert for k_{ei} and ϕ.

4. Conclusions

Guided by recent advances in understanding the basic phase behaviour of polycrystalline ice, and with the aim of providing a rigorous framework within which to analyze paleoclimates as preserved in ice-core records, we have constructed a hierarchy of continuum models to describe the transport of climate proxies in ice sheets. We began by describing a model in which one soluble impurity is sequestered in the premelted liquid network that delineates crystal boundaries and showed that eventually its downward diffusion through the network out-paces the flow of the ice, thereby separating it from the ice with which it was deposited: so-called *anomalous diffusion*. Generalization of this approach to multiple species captures the previous behaviour and displays how compositional diffusion alone can explain the redistribution of peaks in the bulk concentrations of climate proxies. Finally, when we treat the case in which a significant fraction of the total impurity content is not contained in the liquid network, the qualitative aspects, in particular transient effects, of anomalous diffusion are altered.

Acknowledgments

This paper has benefited from ongoing discussions with numerous colleagues; we acknowledge, in particular, the input of Ed Waddington and Grae Worster, and the thoughtful comments of the reviewers. This work is supported by NSF grant No. OPP 9908945.

References

1. W. Dansgaard, S.J. Johnsen, H.B. Clausen et al. Nature (London), **364**, 218 (1993).
2. J.R. Petit, J. Jouzel, D. Raynaud et al. Nature (London), **399**, 429 (1999).
3. T. Blunier and J. Schwander. *In* Physics of ice core records. *Edited by* T. Hondoh. Hokkaido University Press, Hokkaido. 2000. p. 307.
4. S.J. Johnsen, H.B. Clausen, K.M. Cuffey, G. Hoffmann, J. Schwander, and T. Creyts. *In* Physics of ice core records. *Edited by* T. Hondoh. Hokkaido University Press, Hokkaido. 2000. p. 121.
5. J.F. Nye. J. Glaciol. **44**, 467 (1998).
6. A.W. Rempel, E.D. Waddington, J.S. Wettlaufer, and M.G. Worster. Nature (London), **411**, 568 (2001).
7. A.W. Rempel, J.S. Wettlaufer, and E.D. Waddington. J. Geophys. Res. **107**, 2330 (2002).
8. J.F. Nye. J. Glaciol. **37**, 401 (1991).
9. J.G. Dash, H. Fu, and J.S. Wettlaufer. Rep. Prog. Phys. **58**, 115 (1995).
10. J.S. Wettlaufer and J.G. Dash. Sci. Am. **282**, 56 (2000).
11. M.E.R. Walford and J.F. Nye. J. Glaciol. **35**, 107 (1991).
12. J.F. Nye and F.C. Frank. *In* International Association of Scientific Hydrology Publication. IAHS-AISH Publ. No. 107. 1973. p. 157.
13. H.M. Mader. J. Glaciol. **38**, 333 (1992).
14. H. Fukazawa, K. Sugiyama, S. Mae, H. Narita, and T. Hondoh. Geophys. Res. Lett. **25**, 2845 (1998).
15. R. Mulvaney, E.W. Wolff, and K. Oates. Nature (London), **331**, 247 (1988).
16. N.S. Gundestrup, D. Dahl-Jensen, S.J. Johnsen, and A. Rossi. Cold Reg. Sci. Tech. **21**, 399 (1993).
17. J.P. Steffensen, H.B. Clausen, C.U. Hammer, M. Legrand, and M. DeAngelis. J. Geophys. Res. **102**, 26747 (1997).
18. E.C. Pasteur and R. Mulvaney. J. Geophys. Res **105**, 11525 (2000).

19. E.W. Wolff. *In* Chemical exchange between the atmosphere and polar snow. NATO ASI Series I. Vol. 43. *Edited by* E.W. Wolff and R.C. Bales. Springer-Verlag, Berlin. 1996. p. 541.
20. R. Lemlich. J. Colloid Inter. Sci. **64**, 107 (1978).
21. G.W. Gross and R.K. Svec. J. Phys. Chem. **101**, 6282 (1997).
22. I. Baker and D. Cullen. Ann. Glaciol. **35**, (2002). In press.
23. D. Cullen and I. Baker. Microscopy Res. Tech. **55**, 198 (2001).
24. P.R.F. Barnes, R. Mulvaney, E.W. Wolff, and K. Robinson. J. Microscopy, **205**, 118 (2002).
25. P.R.F. Barnes, R. Mulvaney, K. Robinson, and E.W. Wolff. Ann. Glaciol. **35** (2002). In press.